IEEE Access
Multidisciplinary | Rapid Review | Open Access Journal

Received August 15, 2019, accepted September 10, 2019, date of publication September 18, 2019,
date of current version September 30, 2019.

Digital Object Identifier 10.1109/ACCESS.2019.2942058

Planar, Multifunctional 3D Printed Antennas Using Liquid Metal Parasitics

VIVEK T. BHARAMBE[1], (Student Member, IEEE), JINWOO MA[2], MICHAEL D. DICKEY[2], AND JACOB J. ADAMS[1], (Senior Member, IEEE)

[1]Department of Electrical and Computer Engineering, North Carolina State University, Raleigh, NC 27695, USA
[2]Department Chemical and Biomolecular Engineering, North Carolina State University, Raleigh, NC 27695, USA

Corresponding author: Jacob J. Adams (jacob.adams@ncsu.edu)

This work was supported by the U.S. Army Research Office under Grant W911NF-17-1-0216.

ABSTRACT This paper describes a liquid metal-based multifunctional antenna capable of wideband frequency tuning, dual band operation, and polarization reconfiguration. The radiating elements consist of parasitically-excited plugs of room-temperature liquid metal in 3D printed channels. Syringe pumps flow the gallium-alloy plugs in proximity to a capacitive feeding structure. This non-contact feeding scheme separates the metal flow path from the SMA connector and lends mechanical robustness at the feed while allowing impedance matching over a wide range of frequencies. Sliding the plug along a right-angle bend enables linear polarization reconfiguration, while simultaneously placing plugs in both orthogonal channels can generate circular or 45° linear polarization. Dual band operation is also supported by infusing plugs of two dissimilar lengths into the two channels. Simulation and measurement results demonstrate that this antenna can tune its impedance over a decade (10:1 frequency range) maintaining a 2:1 VSWR and achieve a polarization diversity > 12 dB. The pumped plugs can circulate at a peak velocity of 50 mm/s, currently limited only by our pumping equipment. Repeatability analysis is also performed by cycling the plug actuation more than 1100 times. More complex designs can exploit this design concept to develop new types of highly versatile, multi-functional antennas.

INDEX TERMS Reconfigurable antenna, liquid metal antenna, 3D printing, multifunctional antenna, planar antenna, microfluidics.

I. INTRODUCTION

As modern-day antenna systems are growing in complexity, reconfigurability of antenna characteristics such as frequency, pattern or polarization is becoming an important capability. Using electrical switching, mechanical motion or material change based approaches [1], [2], researchers have developed numerous reconfigurable antennas over the past few decades. Furthermore, studies have shown devices in which two [3]–[5] or more [6] antenna properties are reconfigured simultaneously in a single device, making it adaptable for a variety of applications.

Recent approaches for reconfigurable antennas include the use of metal alloys that exist in a liquid state at room temperature and can be reshaped to alter the electromagnetic response of the device. Such fluidically reconfigured antennas have the potential to support a greater number of reconfiguration states than their solid-phase counterparts due to their ability to physically reshape the antenna geometry when changing states. Liquid metal-based reconfiguration techniques have already been demonstrated to exhibit wideband frequency tunability [7], [8], polarization reconfiguration [9], pattern reconfigurability [10], [11], and lower intermodulation distortion than semiconductor-based reconfiguration approaches [12].

However, a number of difficulties arise when developing complex reconfigurable liquid metal (LM) electronics. Foremost among these challenges is enabling flow within microchannels. Gallium alloys, which are often chosen for LM electronics due to their non-toxicity, high conductivity, and low melting point, form a thin oxide layer on their surface even at low oxygen concentration [13]. This oxide skin adheres to the surfaces of most dielectric substrates [14], leaving residues as minute droplets or thin conductive coatings on the channel walls [15]. Consequently, it becomes difficult to circulate the liquid metal inside hollow channels reversibly and repeatably, hampering reliable antenna reconfiguration.

The associate editor coordinating the review of this manuscript and approving it for publication was Davide Comite.

In the literature, many LM-based devices employ concentrated electrolytes to dissolve the skin, and in some cases, to actuate the motion of liquid metal inside the channels [7], [16]. However for antenna implementations, the presence of electrolytes in the channels degrades the antenna radiation efficiency due to their high conductivity [7]. Hence, after cleaning the channels, the electrolytes are sometimes removed before measuring antenna performance [9], [17], which is impractical for most practical scenarios. Moreover, concentrated electrolytes often require special handling, tend to corrode solid metals and hence should be avoided.

In this work, we describe a novel multifunctional LM-based planar antenna that combines 10:1 frequency tuning range and reconfigurable polarization. Practical and repeatable actuation of liquid metal plugs is demonstrated using non-electrolytic fluids. Section II of this paper describes a parasitically driven liquid metal antenna (PLMA) radiating like a microstrip antenna while supporting a wide range of frequency and polarization states. Section III describes fabrication of the multi-channel antenna structure and the methods used to improve liquid metal flow within it. In Section IV, detailed measurement data and analysis confirm that the antenna performs in agreement with simulation and produces among the highest reported tuning range and polarization diversity for compound reconfigurable antennas. Finally in Section V, we study changes in the antenna's response during more than 1000 reconfiguration cycles in order to understand its repeatability, and characterize the plug actuation speeds and limitations of the proposed approach.

II. PARASITICALLY-DRIVEN LIQUID METAL ANTENNA (PLMA) CONCEPT

There are a variety of choices for the antenna geometry upon which to base a reconfigurable LM antenna. Several authors have proposed flowing liquid metal inside capillaries to form reconfigurable monopole or dipole antennas [8], [9], [18], [19]. However, in comparison to microstrip-like geometries, such antennas are more difficult to incorporate onto compact devices that require the antenna to be placed near a ground plane. Integration-friendly rectangular patch antennas using LM have been reported, but it is difficult to control the flow of the metal inside a wide planar cavity, resulting in a non-reconfigurable design [20] or restricting reconfiguration to binary states with fully infused or empty cavities [21]. Planar slot antennas using LM channels to shunt the slots at certain positions have also be studied by a number of authors [22]–[25], but this approach still produces a limited range of states since the liquid metal here functions much like a lumped element switch.

To address the need for multi-functional planar designs that take advantage of the ease of flowing liquid metal inside narrow channels, we propose the narrow fluidic microstrip antenna as shown in Figure 1. The liquid metal acts like a thin microstrip type antenna excited by a capacitively coupled

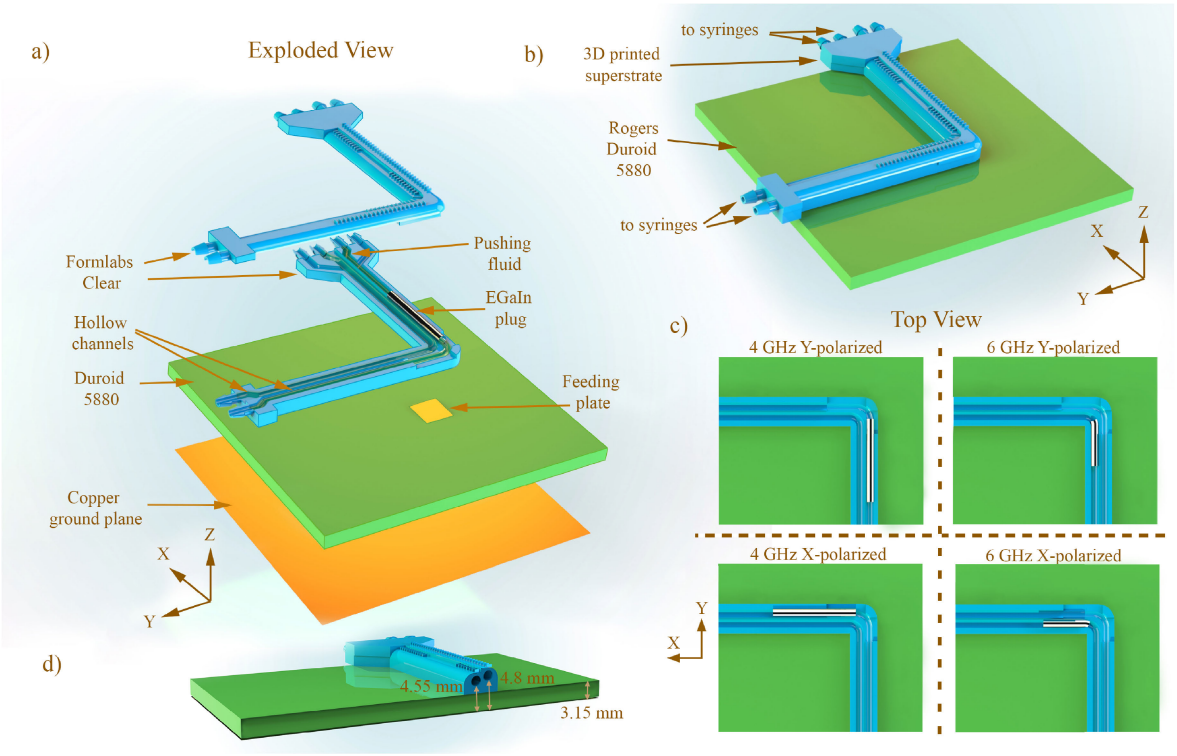

FIGURE 1. a) The exploded view of the antenna structure, demonstrating the substrate and the 3D printed superstrate containing the EGaIn plug, b) The perspective view of the assembled antenna, c) The top view illustrating the location of the EGaIn plug while it is operating at 4 and 6 GHz in vertical and horizontal orientation and d) The cross-sectional view of the antenna showing substrate thicknesses.

feed, in which the length of the antenna can be regulated to operate it at different frequencies while its width is equivalent to the diameter of the fluidic channel.

With such a narrow width, the microstrip antenna has a high impedance when directly fed at the transverse edge. However, the antenna can be readily matched to a 50 Ω source using the proximity coupled feed. Additionally, the parasitic feed prevents direct contact between the pumped liquid metal and the feeding SubMiniature version A (SMA) connector and allows them to exist on separate layers. This minimizes the risk of liquid metal leakage, electrical disconnection, corrosion of the copper, and lends mechanical robustness to liquid metal-rigid SMA interface. Moreover, pump-based actuation eliminates the need for complex DC-RF decoupling circuitry at the feed as required for certain electro-chemical actuation processes [7].

As shown in Figure 1, the proposed antenna geometry consists of a 4.5 mm thick 3D printed part stacked on top of a 3.15 mm RT5880 laminate. A 6 mm x 6 mm square feeding plate is etched on top of the laminate, which connects to the center conductor of the coaxial feed. This excites surface currents along the x, y edges and the diagonal (Figure 2d) on this feeding plate, capable of exciting plugs of either polarization. The back side of this substrate acts a ground plane for the antenna and is soldered to the SMA outer conductor. The L-shaped 3D printed part holding two hollow channels (2 mm diameter) is then attached on top of the laminate at the appropriate location. These channels can be independently filled with EGaIn plugs to form antennas operating at two different frequencies according to the plug length. When positioned on top of the feeding plate as shown in Figure 1, these plugs electromagnetically couple with the feeding plate and operate as microstrip antennas, resonating when their length is approximately half a wavelength inside the 3D printed part ($\lambda_g/2$). As is shown in Section IV, the feed plate alone contributes little radiation and matching the feed to the liquid metal plug is essential.

By choosing an appropriate gap (h) between the resonant plug and the feeding plate and tuning the dimensions of the square feeding plate (s x s mm^2), the input impedance of the antenna structure can be well matched as shown in Figure 2a and b. The real part of the input impedance can be controlled primarily using the feed gap height (h). In addition, the feed gap height will limit the upper and lower tuning range of the antenna because it sets the antenna's electrical thickness. On the other hand, increasing the feed plate size adds series inductance and will eventually limit the upper operating frequency when the feed becomes comparable in size to the resonant plug length.

The design shown in Figure 1 incorporates two distinct channels for frequency reconfiguration. When a 12 mm long EGaIn plug is infused into channel 1, and positioned as shown in Figure 1c, the antenna operates at 6 GHz. Similarly, infusing channel 2 with an 18 mm plug yields a 4 GHz operation. Channel 2 is located obliquely above channel 1. This configuration enables more effective coupling between the feed

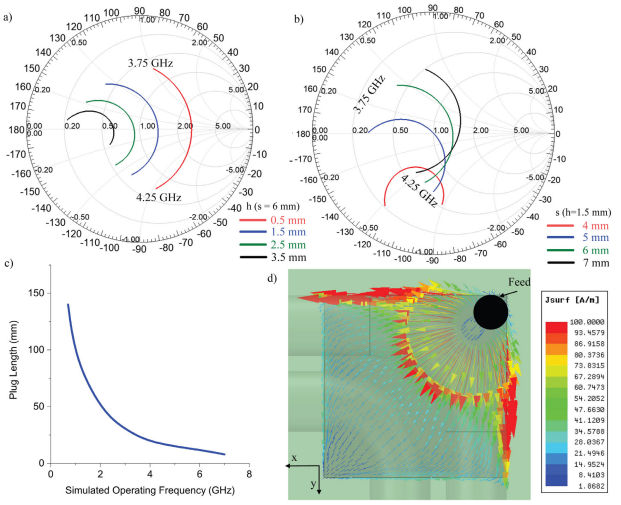

FIGURE 2. a) The simulated S_{11} of the antenna structure for varied height (h) of the EGaIn plug (18 mm long, operating at 4 GHz) above the feeding plate, b) the simulated S_{11} plot of the antenna structure for different feeding plate dimensions for h = 1.5 mm, c) the wide range of operating frequencies achieved by infusing 8-140 mm long EGaIn plugs in channel 1 and d) the simulated surface currents on the feeding plate in absence of a liquid metal plug, illustrating the currents excited on the plate along the x, y edges and the diagonal.

plate and each channel, in contrast with a side-by-side or vertically stacked configuration, which reduces the matching capabilities in one channel. This multi-channel design can be used to achieve frequency reconfiguration, a multi-band response, and both linear and circular polarization as shown in Section IV. Moreover, frequency reconfiguration can also be achieved by infusing EGaIn plugs of varying lengths into either of these channels. For instance, when channel 1 is infused with plugs of lengths 8 - 140 mm, the antenna can be tuned to achieve an operating frequency in the range of 0.7-7 GHz in Figure 2c. Thus the broadband nature of the capacitive coupling between the feeding plate and the plugs allows for a 10:1 frequency range over which this antenna impedance can be tuned using a single channel, assuming a range of plug lengths are available. For all operating frequencies, the planar antenna radiates like a narrow microstrip patch antenna and the peak gain is normal to the ground plane (along the z axis).

Polarization reconfiguration for this antenna can be achieved by sliding the plug of EGaIn over an L-shaped bend that allows it to couple with the symmetrical feed in an orthogonal orientation as shown in Figure 1. Moving the plug along these orthogonal sections enables us to shift between linear x and y polarizations as will be demonstrated in Section IV. To facilitate the transport of EGaIn plugs to specific positions, a non-conductive pushing fluid is essential and we will explore available options in Section III.

III. ANTENNA FABRICATION

A. 3D PRINTING OF THE CHANNELS

3D printing technology can readily build substrates with complex, multilayered channels for enclosing liquid metals [26], [27]. Unlike lamination-based approaches, these uni-body

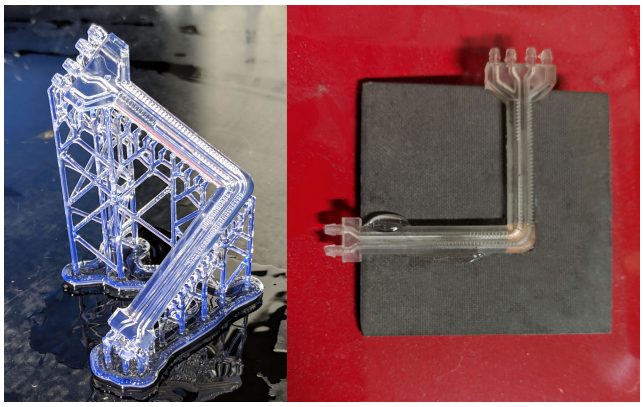

FIGURE 3. a) The 3D printed part (with support structures) containing residual resin inside the hollow channels, which must be removed by flowing IPA and compressed air, and b) The fabricated and assembled antenna.

parts are not prone to leakage of fluids at the lamination interface [21]. However, resins suitable for printing fluidic channels have varying loss characteristics at microwave frequencies. Microfluidic channel fabrication is possible using PolyJet printing based resins like VisiJet M3 Crystal ($\epsilon_r = 3, tan\delta = 0.047$) [28], [29], but they exhibit high dielectric dissipation, reducing the radiation efficiency. Thermoplastics printed using Fused Deposition Modeling (FDM) such as ABSplus ($\epsilon_r = 2.5, tan\delta = 0.0038$) have low loss tangents but microchannel fabrication using FDM has been a known challenge [27]. Stereolithography (SLA) is capable of realizing narrow internal channels with diameters as small as 290 μm [30], with better loss characteristics than PolyJet-based photopolymers. We characterized the electrical permittivity of Formlabs Clear SLA resin ($\epsilon_r = 2.8, tan\delta = 0.021$ at 4 GHz) and observed that it provided a good compromise between achievable microchannel dimensions and dielectric dissipation.

Thus, to build 3D fine-featured microchannels and reduce dielectric losses, we use a mix of conventionally engineered RF substrates and 3D printed parts. Low-loss laminate - Rogers Duroid RT5880 ($\epsilon_r = 2.2, tan\delta = 0.0009$) and 3D printed Formlabs clear resin (RS-F2-GPCL-04) are stacked vertically as shown in Fig 1. The clear resin was printed using SLA-based 3D printer Formlabs Form 2 with a layer thickness of 25 μm. A 405 nm ultraviolet beam selectively cures the resin for each layer and leaves uncured resin inside hollow regions. Clear resin (RS-F2-GPCL-04) allowed visual inspection of the position of EGaIn column inside the channel. The 3D printed part shown in Figure 3 has residual uncured resin on the surface and inside the formed hollow channels. The part was then immersed in an IPA bath for 30 minutes to eliminate residual resin from the outer surface of the printed part. However, this process fails to eliminate the uncured resin from the hollow internal cavities. If allowed to cure, this resin clogs the channels. To prevent this, compressed air was forced through the inlet of the channel after the IPA bath. With the help of syringe pumps, clean IPA was then circulated back-and-forth these channels to eliminate any trace residues. The part was then dried.

B. CHOICE OF LIQUID METAL AND PUSHING FLUIDS

The liquid metal used for this study is the eutectic alloy of gallium and indium - EGaIn (75.5 % Ga and 24.5 % In). With a low melting point of 15.5° C, this alloy exists in a liquid state at room temperature and has an electrical conductivity of $3.4x10^6$ S/m, which is approximately $1/17^{th}$ of that of copper [31]. Plugs of this liquid metal are introduced and steered to form the metallized portion of the reconfigurable antenna geometry.

The pushing fluid both transfers pressure through the channel and may also assist the flow of the sticky oxide skin. Electrolytes have been used in prior work, but their high RF conductivity (5-15 S/m) reduces device efficiency [7], [18]). High viscosity oils have been used to move EGaIn plugs inside channels in the absence of electrolytes [32], and were observed to successfully move EGaIn plugs repeatably if their viscosity was sufficiently high. Furthermore, oils tend to form a lubrication layer on the channel walls, reducing friction and skin adhesion.

Two oils were studied as pushing fluids in this work: silicone oil DMS-T41 (polydimethylsiloxane, trimethylsiloxy terminated, 10,000 cSt, Gelest Inc.) and a blend of oleic acid (Alpha Aersar, A16663) and poly(ethylene vinyl acetate) (EVA, Sigma Aldrich, 340502). The silicone oil was chosen because of its excellent dielectric, thermal and lubricating properties. Oleic acid was chosen because of the ability of gallium surfaces (and alloyed surfaces) to adsorb the primary substituted hydrocarbons, forming an overlayer on the gallium oxide surface [33], [34] as illustrated in Figure 4. Silicone oils such as DMS-T41 are available in a variety of molecular weights and viscosities, but the oleic acid has low viscosity. Hence its viscosity was increased by blending 12g of EVA with 100 ml of oleic acid using a magnetic stirrer and maintaining the solution temperature at 100°C overnight. The resultant 12% EVA blend had a higher viscosity than oleic acid (measured viscosity of 4266 cSt compared to 43.92 cSt initially). In comparison, water has viscosity of 1 cSt, while EGaIn has been reported to have a kinematic viscosity of 0.32 cSt [35].

The electrical permittivity of DMS-T41 ($\epsilon_r = 2.6, tan\delta = 0.008$) and oleic acid ($\epsilon_r = 2.3, tan\delta = 0.014$) were also measured using a resonant cavity method in the 3-6 GHz range. It can easily be observed that the effective RF conductivity ($\sigma_{RF} = 2\pi f \epsilon_0 \epsilon_r tan\delta$) of these fluids at 4 GHz is less than 0.008 S/m (ϵ_0 is the vacuum permittivity) and is orders of magnitude lower than the conductivity of an electrolyte. Furthermore, the electrical permittivity of these fluids is similar to that of the 3D printed substrate, ensuring minimal impact on the design.

C. ASSEMBLY AND FLUID ACTUATION

A 6 mm × 6 mm square feeding plate was etched onto RT5880 laminate. An SMA connector was soldered onto

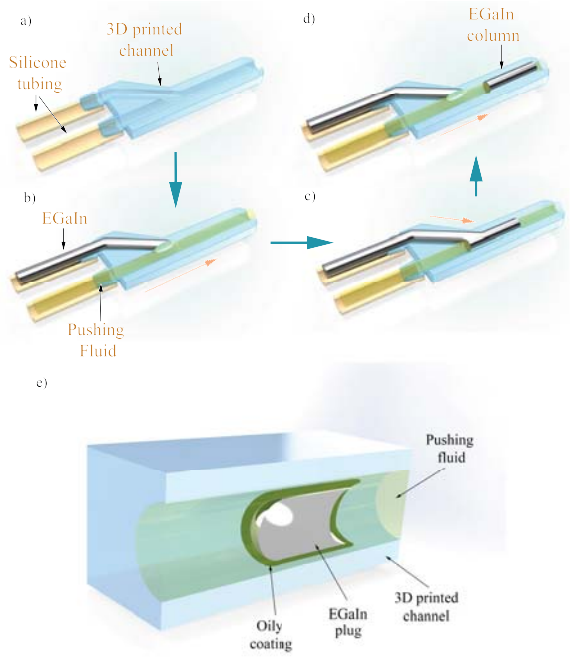

FIGURE 4. a-d) The experimental setup for injecting the EGaIn plugs into the channels. The length of the plugs can be easily controlled by adjusting the time and flow rate of EGaIn infusion in step c, and e) The cross-sectional view of EGaIn plug traversing a 3D printed channel in presence of oleic acid as a pushing fluid.

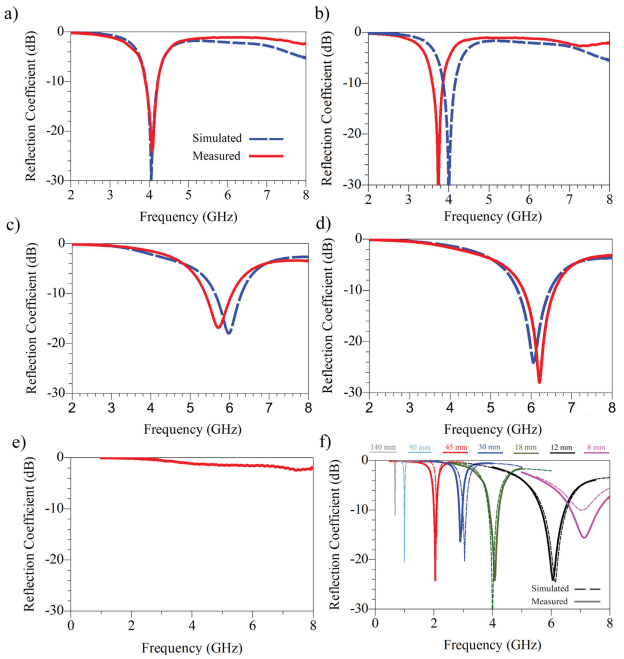

FIGURE 5. Frequency reconfiguration. The measured and simulated reflection coefficient for the EGaIn plugs of length 18 mm in channel 2 in a) x-polarized mode b) y-polarized mode. The reflection coefficient for the EGaIn plugs of length 12 mm in channel 1 for c) x-polarized mode, d) y-polarized mode, e) The measured reflection co-efficient of the antenna in the absence of EGaIn plugs in both the channels, and f) The frequency tuning range achieved by varying the EGaIn plug lengths introduced in channel 1: measured (2-7 GHz) and simulated (0.7-7 GHz) in the x-polarized mode.

the ground plane with its center conductor penetrating the Duroid substrate and connecting to the feeding plate as shown in Figure 3. The 3D printed part was glued on top of the laminate, and silicone tubing (inner diameter 2 mm) was attached via printed connectors to the channels.

Programmable syringe pumps (NE 1600, New Era Pump Systems Inc.) connected to the silicone tubing control the infusion and withdrawal of the fluids. The 2 mm diameter channel is initially filled entirely with the viscous pushing fluid. This helps in developing a slip layer to prevent adhesion of EGaIn to the channel walls. A column of EGaIn is then introduced using a Y-shaped assembly from the EGaIn inlet as shown in the Figure 4. Once the column reaches the necessary length, the other inlet forces pushing fluid into the channel. Syringe pumps on both sides of the channel assist with precise positioning by regulating the infusion/withdrawal of the pushing fluid. This arrangement requires creating and positioning a new LM plug whenever an alteration in length is desired, which is a shortcoming of this approach. Several channels with varying plug lengths can be used, as demonstrated in this work using two adjacent channels, but other methods to allow for rapid changes in plug length are the subject of current investigation.

IV. ANTENNA MEASUREMENTS

The multi-functional structure proposed in Figure 1 is capable of several operating modes. In this section, we report the measured and simulated characteristics of the antenna when performing each of these functions. The measurement conditions are as described in Section III with syringe pumps used to position the LM load in the channel.

A. FREQUENCY RECONFIGURATION

In the absence of EGaIn plugs, the 3D channels are entirely filled with pushing fluid. In this OFF state, the antenna reflects most of the incident power as the feed does not radiate well at this frequency (Figure 5e). When the channels are infused with EGaIn plugs, the structure resonates, leading to a matched response to a 50 Ω source impedance. When channels 1 and 2 are sequentially infused with plugs of lengths 12 mm and 18 mm, the antenna produces a matched response at 6 GHz and 4 GHz, respectively. The agreement between the simulated and measured reflection coefficient as shown in Figure 5 indicates that we can pump plugs of precise lengths and position them properly over the ground plane. For this design, frequency reconfiguration can also be achieved by pumping plugs of different lengths into a single channel. In this way, reconfiguration can be achieved over a wide range of frequencies. As an example, channel 2 was infused with plugs of different lengths (8 mm, 12 mm, 18 mm, 30 mm and 45 mm) to match the antenna at different frequencies ranging from 7 GHz to 2 GHz in discrete steps. The antenna produced a well-matched response, aligning with simulations as shown in Figure 5f. Since the prototype was 80 mm x 80 mm in dimensions, longer plugs of lengths 90 mm and

140 mm were simulated to show that the antenna achieves a 2:1 VSWR bandwidth that is tunable over a decade in frequency. However, as shown in Table 1, the total efficiency begins to decrease rapidly for frequencies below 2 GHz as the dielectric substrate (Duroid and the 3D part) becomes electrically thin ($< \lambda_g/20$). The efficiency of the antenna could be improved by using a lower loss printed material, such as ABSplus, but ultimately the lower band edge will be limited by substrate electrical thickness.

TABLE 1. The realized gain and polarization diversity (PD) at broadside of the fabricated antenna at different frequencies.

Frequency (GHz)	Plug length (mm)	Peak Gain (dBi)	PD (dB)	Simulated Efficiency*	
				Formlabs	ABSplus
7.0	8	5.2*	12*	95%	97%
6.0	12	6.1	14.8	94%	96%
4.0	18	6.2	15.6	86%	95%
3.0	30	5.9	22.6	70%	92%
2.1	45	4.5	33	62%	83%
1.0	90*	1.7*	32*	32%	62%
0.7	140*	-1.5*	19.3*	18%	44%

*Simulated values. Remaining values represent measured data. Results for 1 GHz and 0.7 GHz were simulated by enlarging the lateral dimensions of the Duroid substrate and 3D channels.

B. LINEAR POLARIZATION RECONFIGURATION

Figure 6 shows the radiation patterns of the antenna at 4 and 6 GHz in the x-polarized and y-polarized modes shown in Figure 1. In the 4 GHz x-polarized mode, the antenna produces a co-polar realized gain of 6.2 dBi in comparison to a simulated value of 6.4 dBi. In the y-polarized mode, the measured co-polar realized gain was 6.4 dBi, exactly aligning with simulations. The measured cross-polarized gain was -9.7 dBi for the x-polarized and -12 dBi for the y-polarized mode. This indicates that in switching between two linearly polarized modes by moving the same EGaIn plug through the L-shaped curve, a polarization diversity of 16-18 dB can be achieved at 4 GHz. Because the measured and simulated gains were similar, the simulated total efficiency of 86% at 4 GHz is expected to be a good approximation to the actual antenna efficiency.

Similarly, at 6 GHz, the measured co-polar gain was 6.1 dBi and 6.2 dBi in x and y-polarized mode compared to a simulated value of 6.2 dBi. The polarization diversity degraded by approximately 1 dB to 14.8 dB. At higher frequencies, the polarization diversity reduces (as shown in Table 1) on account of increased magnitude of cross polarized components on the feeding plate, as its electrical size increases. The simulated radiation efficiency at 6 GHz was 94%.

Table 1 illustrates the polarization diversity achieved by switching channel 1 between the x and y polarized modes. A polarization diversity of >12 dB can be achieved at any frequency over a decade. This wide frequency range for a compounded reconfigurability is a significant advance over existing non-fluidic antennas utilizing switches [6], [36], [37]

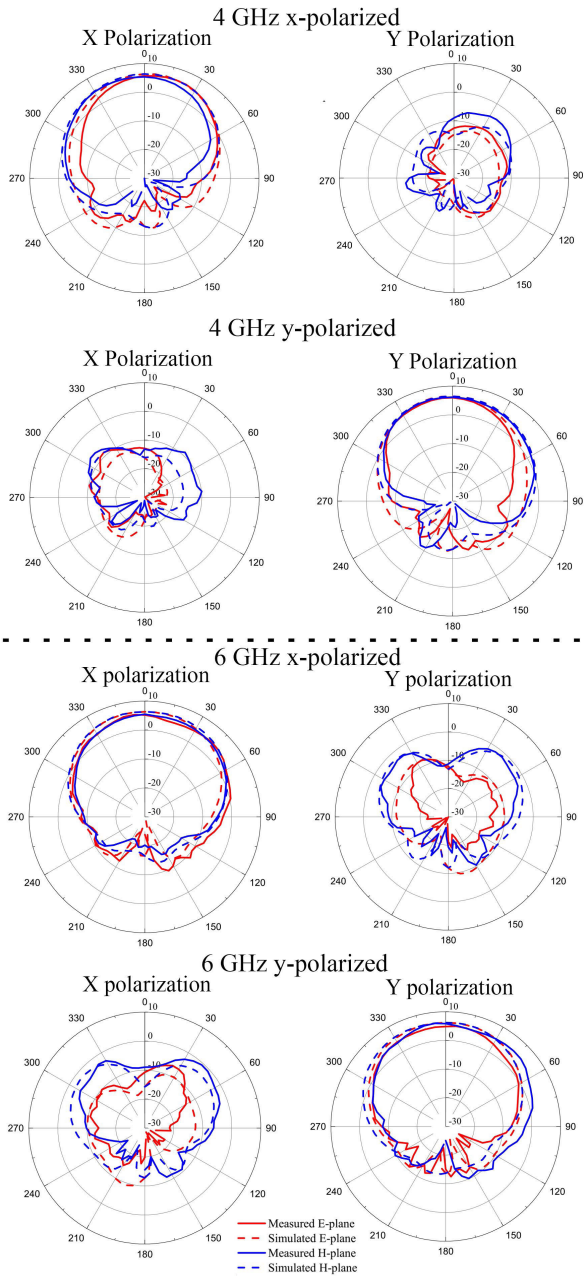

FIGURE 6. Linear polarization reconfiguration. The measured and simulated radiation pattern at 4 GHz and 6 GHz for x and y polarized operating modes. The difference between these states (polarization diversity) is higher than 14 dB in both cases.

and also over existing liquid metal based compound reconfigurable antennas [19] as compared in Table 2.

C. DUAL BAND OPERATION

Filling both the channels with EGaIn plugs of dissimilar lengths enables dual-band operation. Figure 7b illustrates dual band operation by placing two plugs of length 26 mm and 16 mm into channels 1 and 2 in the x-polarized position respectively. We observe two well-matched operating frequencies in the reflection coefficient plot corresponding to

TABLE 2. Performance of selected recently published compound frequency and polarization reconfigurable antennas.

	Freq Range	Size (λ_0)	Radiation Efficiency	Switching Speed	Pol. Diversity
PLMA	10:1	0.33x0.33	18-95%	$< 6s$*	>12 dB
[19]	3.75:1	0.4x0.4	40-70%	<100s	-
[37]	1.67:1	0.33x0.33	-	$< 1\mu s$	>10 dB
[36]	1.4:1	0.5x0.5	25-90%	$< 1\mu s$	>10 dB
[6]	1.21:1	0.6x0.6	45-55%	$< 1\mu s$	-

λ_0 is calculated at the lowest operating frequency of the antenna.
*Measured speed with a 25 mm/s flow rate.

the plug lengths (Figure 7a). The realized gain plots in Figure 7c confirm that both modes are x-polarized with >10 dB polarization purity. It is also evident that despite the close placement of the two radiating plugs, the pattern is not tilted, and the peak gain is in the broadside direction. Likewise, placing the two plugs in the y-orientation simultaneously will produce a y-polarized dual-band response. However, if the two resonances are within the 6 dB bandwidth of each other, a single-band mismatched response is observed. A higher order mode for the 26 mm plug is observed at 6.4 GHz, but the radiation pattern for this mode does not have a peak in the broadside direction.

D. 45° POLARIZATION

When a single plug of twice the length given in Table 1 is moved halfway around the L shaped bend, with both arms symmetric about the feeding plate, the orthogonal x and y polarizations are excited in phase, resulting in a linear polarization at 45° to the principal axes. For example, a 35 mm long plug filling channel 1 as shown in Figure 8b produces a resonance at 4.5 GHz with measured realized gain of 7.7 dBi as shown in Figure 8c. This total gain is 1.5 dB higher than the x or y polarized cases shown above.

E. CIRCULAR POLARIZATION

Combining two linear x and y polarizations also generates circular polarization (CP) using the same antenna structure. When the phase difference between the two arms with orthogonal linear polarization is 90°, the radiated fields are circularly polarized and the axial ratio falls to 0 dB [19]. To achieve the phase quadrature, two methods can be used - tuning the length of the plugs or adjusting their coupling to the feeding plate. The prior approach has been illustrated in [19]. Since the proposed design provides a unique ability to control the coupling of individual plug to the feeding plate, we demonstrate CP using two orthogonally polarized EGaIn plugs of identical length (19.7 mm) in each of the channels as shown in Figure 8. As a result, the antenna achieves a 2:1 VSWR at 3.75 GHz, with a realized gain of 6 dBi and an axial ratio of 1.4 dB at broadside. However, it can be observed from Figure 8f that the range of frequencies over which AR < 3 dB is narrow. This state is difficult to achieve using manually generated plugs because the required precision over the plug length is quite high; thus, we present only simulated data here.

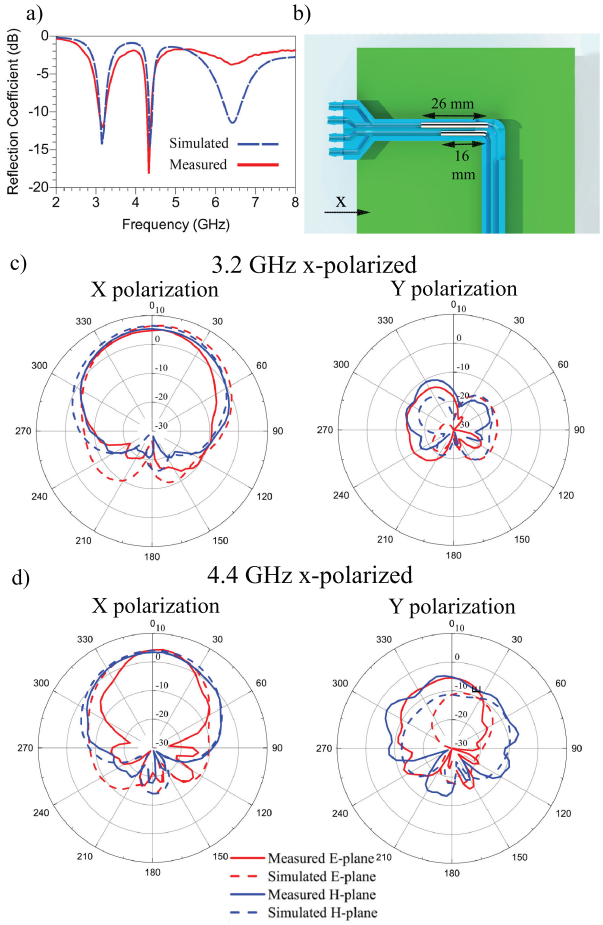

FIGURE 7. Dual-band operation. a) The measured return loss for the dual band antenna demonstrating matched response at 3.2 and 4.4 GHz as predicted by simulations b) the position of the plugs for dual band operation, and the radiation pattern plot of the dual band operating antenna at c) 3.2 GHz and d) 4.4 GHz.

V. SPEED AND REPEATABILITY TESTING

A. ACTUATION SPEED

The time needed to change states is an important metric for any reconfiguration technique. For a semiconductor/MEMS switch-based reconfiguration mechanism, this corresponds to the ON/OFF switching time of the semiconductor/MEMS switch. Reconfiguration speed achieved using these techniques is very fast [1], with diodes and varactors switching times in the order of <100 ns, and MEMS switches achieving $< 250\ \mu s$ transition time. Optical switches are capable of switching faster than 10 μs. However, these switches only modify the material behavior in a localized region of the antenna, in contrast to physically removing materials from the aperture in case of metallic fluids.

Tunable antennas realized using liquid metal displacement such as electrochemically controlled capilarity (ECC) [7] rely on the ability to infuse and withdraw EGaIn using electrochemical changes in surface tension. These approaches have a highly asymmetric actuation profile wherein withdrawal rates are much faster than infusion rates (e.g. 0.6 mm/s [7]),

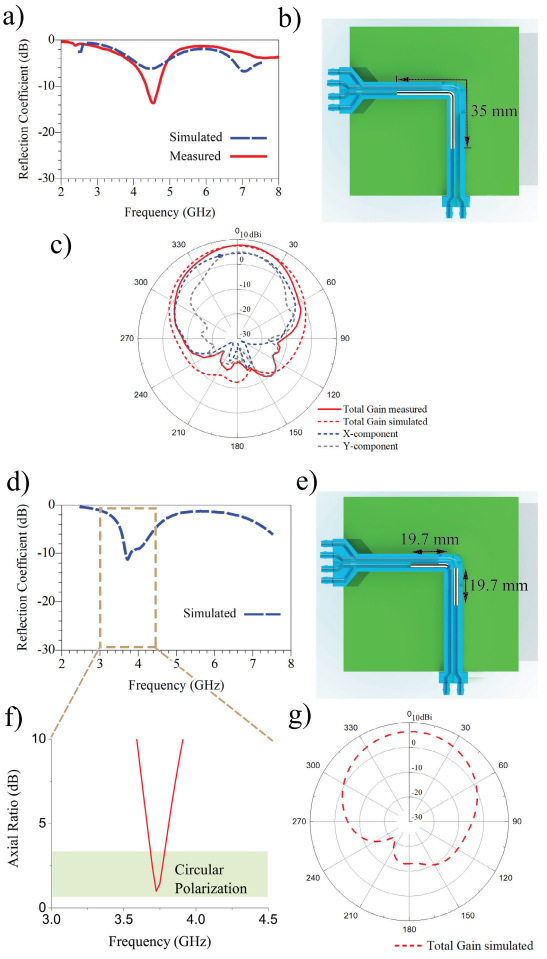

FIGURE 8. Rotated linear and circular polarizations. a) The reflection coefficient for the antenna with a 35 mm plug matched at 4.5 GHz and comparison with simulations, b) the physical alignment of the plug, c) the total measured gain (dBi) for the 45° polarized antenna along with its linear x and y components, d) the simulated reflection coefficient for the circularly polarized antenna with two plugs of 19.7 mm length positioned orthogonally as shown in d), e) the layout for exciting circular polarization using two plugs, and f) the simulated axial ratio value for the antenna demonstrating the narrow range of frequencies over which it is circularly polarized, and g) The simulated total gain (dBi) plot of the circularly polarized antenna at 3.75 GHz.

which ultimately limit the speed of these devices. A number of faster LM-based switching approaches have been proposed including continuous electrowetting-based (CEW) [16], electrowetting on dielectrics (EWOD) [38], and Laplace pressure shaping (LPS) [39]. However, these suffer from a variety of other implementation challenges such as the presence of electrolytes (CEW), high actuation voltage (EWOD), binary switching states (EWOD, LPS), and hermetic sealing to avoid oxidation (LPS).

The reconfiguration speed for our implementation depends on the mobility of EGaIn plugs inside the channels, regulated completely by external syringe pumps. As a result, the plugs can have high mobility and symmetric infusion and withdrawal rates. Since the flow can be controlled by pushing fluids with high dielectric strength and low RF conductivity,

TABLE 3. The plug velocity inside a 2 mm diameter 3D printed channel for different pumping rates.

Syringe Volume (ml)	Internal diameter (mm)	Pumping Rate (ml/min)	Plug Velocity (mm/s)
1	4.7	0.6	3.4
3	8.6	2.02	12.8
30	21.6	10	~50

the performance of RF devices is significantly improved. In previous pump-based implementations, actuation speeds have been low at 0.16 mm/s [11], though these rates are often not reported in the electronics literature. However, analytical calculations have demonstrated that it can be as high as 1.2 m/s for microfluidic channels [40].

To characterize the plug velocities for our setup, we used two pumps - an infusing pump and a withdrawing pump at either end of the channel shown in Figure 1. These pumps move the pushing fluid inside the channel at the same rate, causing the plug to move back and forth. Using syringes of different volumes allowed varied pumping rates as shown in Table 3. The speed of the plug inside a 2 mm 3D printed channel was monitored using a camera. The peak plug velocity was observed to be roughly 50 mm/sec when using a 30 ml syringe with pumping rate of 10 ml/min. At the peak speed, the plug maintained its shape and no residues were observed on the channel walls. The maximum pumping rate was limited by the equipment for our setup and higher plug velocities may be achievable by using different pumps, higher capacity syringes or flowing plugs inside narrower channels. With a plug velocity of 50 mm/s, a plug operating at 6 GHz (12 mm) would take roughly 250 ms to switch between the two linear polarizations. However, since some time is spent in accelerating the plug to the peak velocity, the resultant switching time will be higher. Nevertheless, a switching time in the order of a few hundreds of milliseconds appears feasible with this approach. Compact pumps can also be used, but trade-offs related to switching speed, weight and volume need to be assessed as per specific antenna integration requirements.

B. REPEATED ACTUATION: RESIDUES, DEBRIS AND PLUG SPLITTING

While liquid metal actuation allows reconfigurability, the device must also be able to repeat the actuation many times without needing to clean the channels. Most studies to date require frequent flushing with electrolytes to clean the channels or neglect the repeatability aspect entirely. However, one recent study cycled the actuation of an EGaIn droplet 100 times showing that the reported RF switch remained operational despite small residues [32]. For our study, the repeatability of the plug actuation was tested by cycling it reversibly inside the 3D printed channels hundreds of times. Intermittently, the reflection coefficient of the antenna and its pattern were measured to detect any deviations in its response.

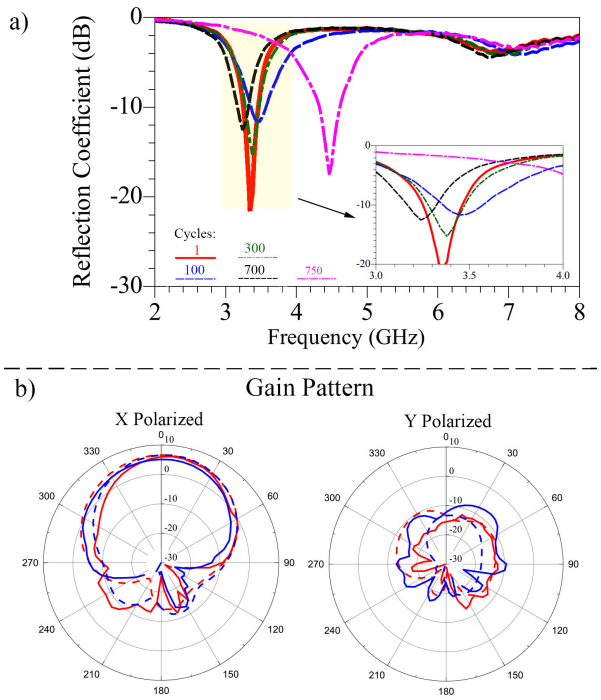

FIGURE 9. a) The measured reflection coefficient for the same plug cycled after 1, 100, 300, 700 and 750 times, and b) The radiation pattern of the antenna after cycling the plug 300 times, well aligned with the pattern of simulated antenna model without any debris.

Due to the presence of the slip layer formed by the viscous pushing fluid, EGaIn did not adhere to the channel walls and hence, residues were not observed. However, the presence of pushing fluids lead to the formation of debris composed of EGaIn skin flakes and EGaIn micro-droplets suspended inside the pushing fluid. When the EGaIn plug was cycled as few as six times with DMS-T41 surrounding it, a significant amount of debris were observed dispersed inside the pushing fluid. The debris was reduced when using oleic acid, where similar amount of debris appeared after 20 repetitions. However, debris accumulate using either fluid as the number of cycles are increased.

Despite the presence of debris, the reflection coefficient measurements taken after 100, 300 cycles and the radiation pattern plots after 300 cycles (Figure 9 show that the debris have negligible impact on antenna performance. Furthermore, Table 4) shows that the matched bandwidth is stable over hundreds of cycles.

During the first cycling experiment, the plug was moved back-and-forth 700 times before it split into two distinct plugs of smaller lengths causing the antenna to operate at 4.5 GHz as shown in Figure 9a and 10c. The debris generated was removed from the channels and collected inside the petri dish (Figure 10b). In the second experiment, the plug was cycled 1100 times before ending due to a pump failure. At the end of the experiment, the plug was intact and the antenna maintained its operating frequency. This demonstrates that, despite the formation of debris, the oleic acid and EVA solution

TABLE 4. The 2:1 VSWR bandwidth observed from reflection coefficient measurements taken after various repetition cycles.

Cycle	f_h	f_l	Bandwidth
1	3.461	3.251	0.21
100	3.571	3.359	0.212
300	3.479	3.279	0.2
700	3.323	3.165	0.158

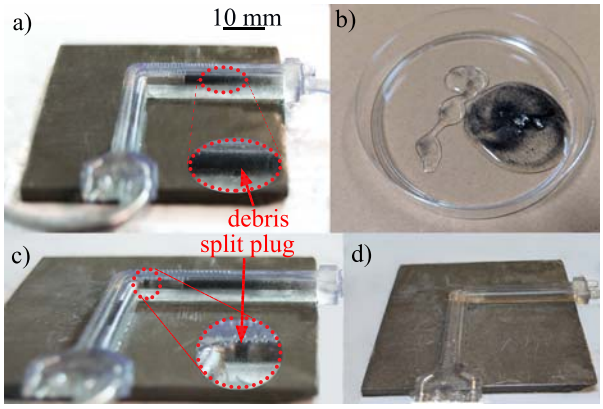

FIGURE 10. a) The black colored debris generated on cycling the plug repeatedly, b) Removing the debris from the channels demonstrating that it consists of oxide skin and micro-droplets of EGaIn, c) Image illustrating the split plug after 750 cycles, and d) Flowing additional pushing fluid through the channel eliminates all debris.

can cycle the EGaIn for a large number of cycles, before the channels must be flushed. The lack of residues on the walls facilitates a thorough cleaning of the channels as shown in Figure 10d. When the same test was performed on 3D printed channels with oxide-phobic coatings [41], the debris were still observed after a number of cycles, illustrating that such coatings are effective in reducing residues but not the debris.

C. ANTENNA ORIENTATION

The actuation of the EGaIn plug of the antenna was tested in both vertical and horizontal orientation. Due to the high viscosity of the pushing fluid and low channel diameter, the actuation of the device was well-controlled in both the orientations. In addition, when the plug was placed in a sealed channel vertically, with the pushing fluid at the bottom and the top, the plug remained intact and stationary against gravity for ~36 hours of observation time.

VI. CONCLUSION

Through controlled flow of liquid metal plugs, we have demonstrated the a multifunctional planar antenna with widely varying frequency and radiation characteristics. By moving a plug of controlled length into the near field of the capacitive coupling element, the operating frequency of the antenna can be tuned over a very wide 10:1 frequency range while maintaining a 2:1 VSWR. At the same time, flowing plugs into orthogonal sections of the geometry, polarization diversity can be achieved. Moreover, we proposed a novel pushing solution of oleic acid and EVA that both reduce

channel resides and oxide debris. Finally, the device was cycled over 700 times with stable performance. This study raises prospects for designing practical and efficient multifunctional antennas with an extremely versatile range of states. 3D printing advances continue to enable more intricate microfludic channels, allowing us to build more complex and faster switching designs in the future.

ACKNOWLEDGMENT

The authors would like to thank Rogers Corp. for providing dielectric substrates, Dr. Jesse Jur, James. B. Hunt library makerspace facility for assistance with 3D printing and Matthew J. Slater for discussions leading to the conceptualization of this design.

REFERENCES

[1] C. G. Christodoulou, Y. Tawk, S. A. Lane, and S. R. Erwin, "Reconfigurable antennas for wireless and space applications," *Proc. IEEE*, vol. 100, no. 7, pp. 2250–2261, Jul. 2012.

[2] J. T. Bernhard, "Reconfigurable antennas," *Synth. Lect. Antennas*, vol. 2, no. 1, pp. 1–66, Jan. 2007.

[3] M. J. Slater, H. K. Pan, and J. T. Bernhard, "Preliminary results in the development of a compound reconfigurable antenna," in *Proc. IEEE Antennas Propag. Soc. Int. Symp.*, Jul. 2008, pp. 1–4.

[4] G. H. Huff, J. Feng, S. Zhang, and J. T. Bernhard, "A novel radiation pattern and frequency reconfigurable single turn square spiral microstrip antenna," *IEEE Microw. Wireless Compon. Lett.*, vol. 13, no. 2, pp. 57–59, Feb. 2003.

[5] S. Nikolaou, C. Lugo, I. Carrasquillo, D. C. Thompson, G. E. Ponchak, J. Papapolymerou, and M. M. Tentzeris, "Pattern and frequency reconfigurable annular slot antenna using PIN diodes," *IEEE Trans. Antennas Propag.*, vol. 54, no. 2, pp. 439–448, Feb. 2006.

[6] D. Rodrigo, B. A. Cetiner, and L. Jofre, "Frequency, radiation pattern and polarization reconfigurable antenna using a parasitic pixel layer," *IEEE Trans. Antennas Propag.*, vol. 62, no. 6, pp. 3422–3427, Jun. 2014.

[7] M. Wang, C. Trlica, M. R. Khan, M. D. Dickey, and J. J. Adams, "A reconfigurable liquid metal antenna driven by electrochemically controlled capillarity," *J. Appl. Phys.*, vol. 117, no. 19, May 2015, Art. no. 194901. [Online]. Available: http://scitation.aip.org/content/aip/journal/jap/117/19/10.1063/1.4919605

[8] A. Dey, R. Guldiken, and G. Mumcu, "Microfluidically reconfigured wideband frequency-tunable liquid-metal monopole antenna," *IEEE Trans. Antennas Propag.*, vol. 64, no. 6, pp. 2572–2576, Jun. 2016.

[9] G. B. Zhang, R. C. Gough, M. R. Moorefield, K. J. Cho, A. T. Ohta, and W. A. Shiroma, "A liquid-metal polarization-pattern-reconfigurable dipole antenna," *IEEE Antennas Wireless Propag. Lett.*, vol. 17, pp. 50–53, Jan. 2018.

[10] A. M. Morishita, C. K. Y. Kitamura, A. T. Ohta, and W. A. Shiroma, "A liquid-metal monopole array with tunable frequency, gain, and beam steering," *IEEE Antennas Wireless Propag. Lett.*, vol. 12, pp. 1388–1391, 2013.

[11] D. Rodrigo, L. Jofre, and B. A. Cetiner, "Circular beam-steering reconfigurable antenna with liquid metal parasitics," *IEEE Trans. Antennas Propag.*, vol. 60, no. 4, pp. 1796–1802, Apr. 2012.

[12] M. Wang, I. M. Kilgore, M. B. Steer, and J. J. Adams, "Characterization of intermodulation distortion in reconfigurable liquid metal antennas," *IEEE Antennas Wireless Propag. Lett.*, vol. 17, no. 2, pp. 279–282, Feb. 2018.

[13] T. Liu, P. Sen, and C.-J. Kim, "Characterization of nontoxic liquid-metal alloy galinstan for applications in microdevices," *J. Microelectromech. Syst.*, vol. 21, no. 2, pp. 443–450, Apr. 2012.

[14] M. R. Khan, C. Trlica, J.-H. So, M. Valeri, and M. D. Dickey, "Influence of water on the interfacial behavior of gallium liquid metal alloys," *ACS Appl. Mater. Interfaces*, vol. 6, no. 24, pp. 22467–22473, Dec. 2014. doi: 10.1021/am506496u.

[15] M. R. Khan, C. Trlica, and M. D. Dickey, "Recapillarity: Electrochemically controlled capillary withdrawal of a liquid metal alloy from microchannels," *Adv. Funct. Mater.*, vol. 25, no. 5, pp. 671–678, Feb. 2015. [Online]. Available: https://onlinelibrary.wiley.com/doi/abs/10.1002/adfm.201403042

[16] J. Lee and C.-J. Kim, "Surface-tension-driven microactuation based on continuous electrowetting," *J. Microelectromech. Syst.*, vol. 9, no. 2, pp. 171–180, Jun. 2000.

[17] G. H. Huff, H. Pan, D. J. Hartl, G. J. Frank, R. L. Bradford, and J. W. Baur, "A physically reconfigurable structurally embedded vascular antenna," *IEEE Trans. Antennas Propag.*, vol. 65, no. 5, pp. 2282–2288, May 2017.

[18] M. Wang, "Electrically controlled liquid metal antennas and periodic structures," Ph.D. dissertation, Dept. Elect. Eng., North Carolina State Univ., Raleigh, NC, USA, 2017.

[19] M. Wang, M. R. Khan, M. D. Dickey, and J. J. Adams, "A compound frequency- and polarization- reconfigurable crossed dipole using multi-directional spreading of liquid metal," *IEEE Antennas Wireless Propag. Lett.*, vol. 16, pp. 79–82, 2017.

[20] G. J. Hayes, J.-H. So, A. Qusba, M. D. Dickey, and G. Lazzi, "Flexible liquid metal alloy (EGaIn) microstrip patch antenna," *IEEE Trans. Antennas Propag.*, vol. 60, no. 5, pp. 2151–2156, May 2012.

[21] V. Bharambe, J. J. Adams, I. D. Joshipura, H. R. Ayers, and M. D. Dickey, "Reversibly reconfigurable liquid metal patch antenna using a superhydrophobic spray-coating," in *Proc. IEEE Int. Symp. Antennas Propag. USNC/URSI Nat. Radio Sci. Meeting*, Jul. 2018, pp. 287–288.

[22] R. C. Gough, J. H. Dang, A. M. Morishita, A. T. Ohta, and W. A. Shiroma, "Frequency-tunable slot antenna using continuous electrowetting of liquid metal," in *IEEE MTT-S Int. Microw. Symp. Dig.*, Jun. 2014, pp. 1–4.

[23] A.-P. Saghati, J.-S. Batra, J. Kameoka, and K. Entesari, "Miniature and reconfigurable CPW folded slot antennas employing liquid-metal capacitive loading," *IEEE Trans. Antennas Propag.*, vol. 63, no. 9, pp. 3798–3807, Sep. 2015.

[24] L. Song, W. Gao, C. O. Chui, and Y. Rahmat-Samii, "Liquid metal 3D printed microfluidic channel reconfigurable patch antenna with switchable slots," in *Proc. United States Nat. Committee URSI Nat. Radio Sci. Meeting (USNC-URSI NRSM)*, Jan. 2018, pp. 1–2.

[25] M. Kelley, C. Koo, H. Mcquilken, B. Lawrence, S. Li, A. Han, and G. Huff, "Frequency reconfigurable patch antenna using liquid metal as switching mechanism," *Electron. Lett.*, vol. 49, no. 22, pp. 1370–1371, Oct. 2013.

[26] R. D. Sochol, E. Sweet, C. C. Glick, S.-Y. Wu, C. Yang, M. Restaino, and L. Lin, "3D printed microfluidics and microelectronics," *Microelectron. Eng.*, vol. 189, pp. 52–68, Apr. 2018. [Online]. Available: http://www.sciencedirect.com/science/article/pii/S0167931717304070

[27] N. Bhattacharjee, A. Urrios, S. Kang, and A. Folch, "The upcoming 3D-printing revolution in microfluidics," *Lab Chip*, vol. 16, no. 10, pp. 1720–1742, May 2016. [Online]. Available: http://pubs.rsc.org/en/content/articlelanding/2016/lc/c6lc00163g

[28] V. Bharambe, D. P. Parekh, C. Ladd, K. Moussa, M. Dickey, and J. J. Adams, "Liquid-metal-filled 3-D antenna array structure with an integrated feeding network," *IEEE Antennas Wireless Propag. Lett.*, vol. 17, no. 8, pp. 739–742, May 2018.

[29] V. Bharambe, D. P. Parekh, C. Ladd, K. Moussa, M. D. Dickey, and J. J. Adams, "Vacuum-filling of liquid metals for 3D printed RF antennas," *Additive Manuf.*, vol. 18, pp. 221–227, Dec. 2017. [Online]. Available: http://www.sciencedirect.com/science/article/pii/S2214860417301525

[30] Q. Ji, J. M. Zhang, Y. Liu, X. Li, P. Lv, D. Jin, and H. Duan, "A modular microfluidic device via multimaterial 3D printing for emulsion generation," *Sci. Rep.*, vol. 8, no. 1, Mar. 2018, Art. no. 4791. [Online]. Available: https://www.nature.com/articles/s41598-018-22756-1

[31] M. D. Dickey, R. C. Chiechi, R. J. Larsen, E. A. Weiss, D. A. Weitz, and G. M. Whitesides, "Eutectic gallium-indium (EGaIn): A liquid metal alloy for the formation of stable structures in microchannels at room temperature," *Adv. Funct. Mater.*, vol. 18, no. 7, pp. 1097–1104, Apr. 2008. [Online]. Available: http://onlinelibrary.wiley.com/doi/10.1002/adfm.200701216/abstract

[32] C. Koo, B. E. LeBlanc, M. Kelley, H. E. Fitzgerald, G. H. Huff, and A. Han, "Manipulating liquid metal droplets in microfluidic channels with minimized skin residues toward tunable RF applications," *J. Microelectromech. Syst.*, vol. 24, no. 4, pp. 1069–1076, Aug. 2015.

[33] S. P. Pujari, L. Scheres, A. T. M. Marcelis, and H. Zuilhof, "Covalent surface modification of oxide surfaces," *Angew. Chem. Int. Ed.*, vol. 53, no. 25, pp. 6322–6356, 2014. [Online]. Available: https://onlinelibrary.wiley.com/doi/abs/10.1002/anie.201306709

[34] C. M. De Silva, B. Pandey, F. Li, and T. Ito, "Adsorption of primary substituted hydrocarbons onto solid gallium substrates," *Langmuir*, vol. 29, no. 14, pp. 4568–4573, Apr. 2013.

[35] J. N. Koster, "Directional solidification and melting of eutectic GaIn," *Cryst. Res. Technol.*, vol. 34, no. 9, pp. 1129–1140, 1999.
[36] N. Nguyen-Trong, L. Hall, and C. Fumeaux, "A frequency- and polarization-reconfigurable stub-Loaded microstrip patch antenna," *IEEE Trans. Antennas Propag.*, vol. 63, no. 11, pp. 5235–5240, Nov. 2015.
[37] P.-Y. Qin, Y. J. Guo, Y. Cai, E. Dutkiewicz, and C.-H. Liang, "A reconfigurable antenna with frequency and polarization agility," *IEEE Antennas Wireless Propag. Lett.*, vol. 10, pp. 1373–1376, Dec. 2011.
[38] P. Sen and C. J. Kim, "A fast liquid-metal droplet microswitch using EWOD-driven contact-line sliding," *J. Microelectromech. Syst.*, vol. 18, no. 1, pp. 174–185, Feb. 2009.
[39] B. L. Cumby, G. J. Hayes, M. D. Dickey, R. S. Justice, C. E. Tabor, and J. C. Heikenfeld, "Reconfigurable liquid metal circuits by Laplace pressure shaping," *Appl. Phys. Lett.*, vol. 101, no. 17, Oct. 2012, Art. no. 174102. [Online]. Available: http://aip.scitation.org.prox.lib.ncsu.edu/doi/abs/10.1063/1.4764020
[40] D. J. Hartl, G. J. Frank, R. J. Malak, and J. W. Baur, "A liquid metal-based structurally embedded vascular antenna: II. Multiobjective and parameterized design exploration," *Smart Mater. Struct.*, vol. 26, no. 2, Dec. 2016, Art. no. 025002.
[41] I. D. Joshipura, H. R. Ayers, G. A. Castillo, C. Ladd, C. E. Tabor, J. J. Adams, and M. D. Dickey, "Patterning and reversible actuation of liquid gallium alloys by preventing adhesion on rough surfaces," *ACS Appl. Mater. Interfaces*, vol. 10, no. 51, pp. 44686–44695, Dec. 2018. [Online]. Available: https://pubs.acs.org/doi/abs/10.1021/acsami.8b13099

VIVEK T. BHARAMBE received the B.E. degree in electronics and telecommunication engineering from Mumbai University, in 2014, and the M.S. degree in electrical engineering from North Carolina State University, in 2017, where he is currently pursuing the Ph.D. degree in electrical engineering. His research interests include reconfigurable antennas, phased arrays, novel materials, stretchable electronics, and 3D printed RF/microwave devices.

JINWOO MA received the B.S. degree in materials science and engineering with Seoul National University, in 2012. He is currently pursuing the Ph.D. degree in materials science and engineering with Seoul National University, and is also a Visiting Scholar with North Carolina State University. His research interests include patterning and actuating liquid metals for flexible and stretchable electronics, and actuating soft materials by harnessing smart polymers and interfacial bonding.

MICHAEL D. DICKEY received the B.S. degree in chemical engineering from the Georgia Institute of Technology, in 1999, and the Ph.D. degree in chemical engineering from The University of Texas at Austin, in 2006, under the guidance of Prof. G. Willson. From 2006 to 2008, he was a Postdoctoral Fellow of the lab of Prof. G. Whitesides at Harvard University. In August 2008, he joined the Department of Chemical and Biomolecular Engineering, NC State University, where he is currently the Alcoa Professor and Alumni Distinguished Undergraduate Professor. He completed a sabbatical at Microsoft, in 2016. His research interests include patterning and actuating soft materials by studying and harnessing thin films, interfaces, and unconventional fabrication techniques.

JACOB J. ADAMS received the B.S. and M.S. degrees in electrical engineering from Ohio State University, in 2005 and 2007, respectively, and the Ph.D. degree from the University of Illinois at Urbana–Champaign, in 2011. From 2011 to 2012, he was an Intelligence Community Postdoctoral Research Associate with the University of Illinois. Since 2013, he has been with the Department of Electrical and Computer Engineering, North Carolina State University, where he is currently an Associate Professor. His research interests include electrically small and reconfigurable antennas, characteristic mode theory, time-modulated antennas, and novel materials and fabrication methods for microwave devices. He was a recipient of several national awards including the DARPA Young Faculty Award, the U.S. Army Research Office Young Investigator Award, and the NSF Graduate Research Fellowship.